

Automated Quantitative Analysis of HDM2 Expression in Malignant Melanoma Shows Association with Early-Stage Disease and Improved Outcome

Aaron J. Berger,¹ Robert L. Camp,¹ Kyle A. DiVito,¹ Harriet M. Kluger,² Ruth Halaban,³ and David L. Rimm¹

Departments of ¹Pathology, ²Medicine, and ³Dermatology, Yale University School of Medicine, New Haven, Connecticut

ABSTRACT

The incidence of cutaneous malignant melanoma continues to increase every year, and this disease remains the leading cause of skin cancer death in industrialized countries. Despite the aggressive nature of advanced melanoma, there are no standard biological assays in clinical usage that can predict metastasis. This may be due, in part, to the inadequacy of reproducible assessment of protein expression using traditional immunohistochemistry. We have previously described a novel method of quantitative assessment of protein expression (AQUA) with the continuity and accuracy of an ELISA assay but with maintenance of critical spatial information. Here, we modify this technology for the evaluation of protein expression in melanoma. Using a tissue microarray cohort of 405 melanoma lesions and 17 normal skin samples, we analyzed expression of HDM2, the human homologue of murine double minute 2 with automated quantitative analysis. We show that expression levels in the nucleus are significantly higher in primary melanomas than in metastatic lesions. Furthermore, high levels of expression are predictive of better outcome. This study demonstrates that quantitative assessment of protein expression is useful in melanoma to validate potential tissue biomarkers and suggests that human homologue of murine double minute 2 may be a valuable prognostic tool for management of malignant melanoma.

INTRODUCTION

Malignant melanoma is currently the malignancy with the most rapid increase in incidence in the United States (1, 2). The fifth most common cancer (3), melanoma is the most common fatal malignancy among young adults (4), with 53,600 new cases diagnosed in 2002 (5). Current estimates predict that 1 in 71 individuals will develop melanoma during their lifetime, up from an initial estimate of 1 in 600 in 1960 and 1 in 150 in 1985 (1).

A number of clinical and pathological factors have been described as markers of prognosis in cutaneous malignant melanoma; however, there are currently no routinely used, broadly accepted molecular, or immunohistochemical markers to define subsets of this neoplasm (6) or predict outcome. The current methods of prognosis in cutaneous melanoma have not changed much since the 1970s when Breslow (7) and Clark *et al.* (8) first published reports indicating the importance of dermal invasion in prognosis. The models of Breslow and Clark remain the most powerful and reliable predictors of survival in primary melanoma (9), despite the molecular revolution of the past 30 years.

To develop a better understanding of melanoma biology and development, as well as discover molecular markers of potential benefit

in melanoma prognosis, a number of studies have evaluated immunohistochemical markers on an individual basis and in numerous relatively small cohorts. Very few, however, have been performed on melanoma tissue microarrays (10, 11), and none have made use of quantitative analysis. Differences in expression levels in the tissues have been limited to those that are easily detectable by the human eye. The current immunohistochemical technology is susceptible to high levels of inter- and intraobserver variability and fraught with variability as a function of the lack of standardization of antibody-based techniques (12–14).

Tissue microarrays provide a highly efficient and economical way to evaluate hundreds of tumors on a single slide (15). The use of tissue microarray technology eliminates the slide-to-slide variability inherent to immunohistochemical methods because all tissues are present on the same slide and are exposed to the same experimental conditions. The use of archival tissues allows for a retrospective study with the benefit of long-term patient follow-up. In addition to improving our understanding of key molecular events in cancer progression, tissue microarrays provide an excellent mechanism for the discovery of outcome predictor models, particularly when coupled with quantitative analysis.

We have developed a system for compartmentalized, automated quantitative analysis of histologic sections (16). This system, called AQUA, provides highly reproducible analysis of target signal expression in tissues on a continuous scale while preserving spatial information, particularly subcellular localization. Quantitative analysis enables precise discrimination of expression levels in tissues, providing measurements on a continuous scale not previously attainable by traditional or manual scoring methods. The use of this technology was originally described in colon cancer (16) and has since been applied to breast (17) and prostate (18) carcinoma. Briefly, the system identifies and tags tumor tissue within each histospot based on the expression of tissue-specific proteins such as cytokeratin in carcinomas and then evaluates the expression level of a target antigen within the tumor mask and inside user-defined subcellular compartments. For this study, the automated quantitative analysis system was modified to accommodate melanoma by substituting S100 protein for cytokeratin (Fig. 1). A review of the pertinent literature demonstrated that S100 is expressed in 97.4% of all melanomas (19), and some investigators suggest this number may exceed 98% (20). Here, we validate the technology by assessing the expression of human homologue of murine double minute 2 (HDM2) and demonstrate its use in evaluating a prognostic marker in a large retrospective cohort.

HDM2 is a transcriptional target of the tumor suppressor protein p53 that, in turn, marks p53 for degradation (21–23). It is predicted that disruption of this negative feedback loop, through either p53 mutation or overexpression of HDM2, would be a negative prognostic marker for cancer progression. The association between HDM2 and clinical outcome has been investigated intensively in a number of cancers (24) with the anticipation of using HDM2 as a clinical prognostic marker. However, only a handful of studies have evaluated HDM2 expression in melanoma (10, 25, 26). In the largest study, Polsky *et al.* (27) demonstrated that overexpression of HDM2 in a cohort of 134 melanoma patients unexpectedly correlated with improved clinical outcome, having a statistically significant association

Received 4/20/04; revised 8/24/04; accepted 9/16/04.

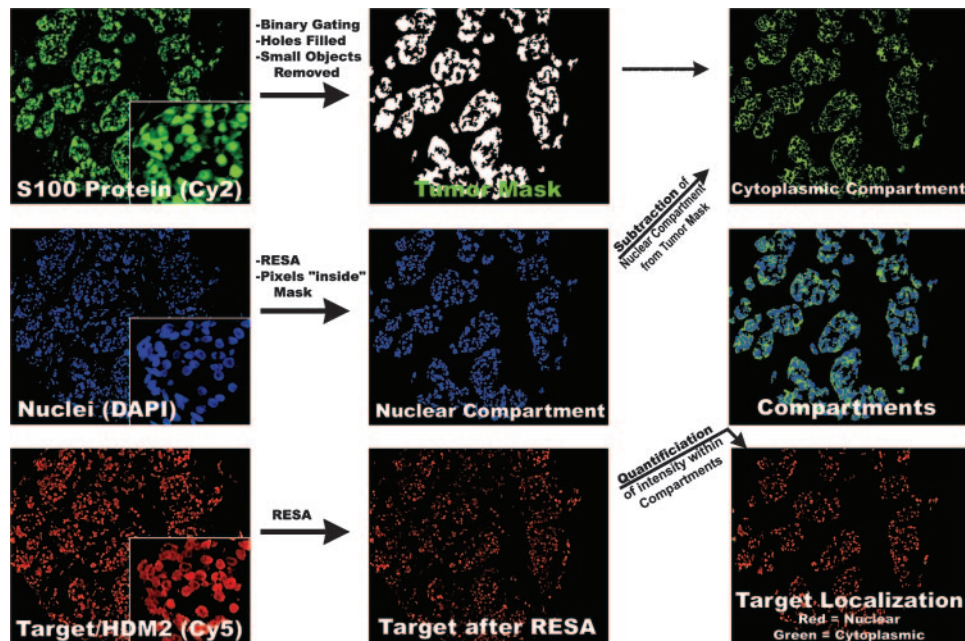
Grant support: NIH/National Institute of General Medical Sciences Medical Scientist Training Program Grant GM07205 (A. Berger), NIH Grant K0-8 ES11571 (R. Camp), C. J. Swebilius Award for Translational Research and the Ethel F. Donaghy Foundation for Women's Health Research at Yale (H. Kluger), USPHS Grant CA44542 (R. Halaban), the Patrick and Catherine Weldon Donaghy Foundation for Medical Research (D. Rimm), and NIH Grant R21 CA 100825 and United States Army Grant DAMD-17-02-0463.

The costs of publication of this article were defrayed in part by the payment of page charges. This article must therefore be hereby marked *advertisement* in accordance with 18 U.S.C. Section 1734 solely to indicate this fact.

Requests for reprints: David L. Rimm, Department of Pathology, Yale University School of Medicine, P. O. Box 20803, 310 Cedar Street, New Haven, CT 06520. Phone: (203) 737-4204; E-mail: david.rimm@yale.edu.

©2004 American Association for Cancer Research.

Fig. 1. Schematic demonstration of the AQUA protocol applied to melanoma. Images on the left are raw. Images on the right have been generated by automated quantitative analysis. The top horizontal set of panels demonstrates tumor mask in a melanoma histospot based on S100 protein expression (Alexa 488), distinguishing tumor cells from stroma. The S100 image is gated to form a binary mask. This binary image is enhanced by filling holes and removing small objects. A 4',6-Diamidino-2-phenylindole (DAPI) is used to tag the nuclei, and after application of rapid exponential subtraction algorithm (RESA) and identification of only those pixels within the tumor mask, this image designates the nuclear compartment. After application of RESA to the Alexa 488 image, the nuclear compartment is subtracted from the tumor mask to provide a designation of the cytoplasmic compartment. An image of the target-specific marker HDM2 is taken (Cy5), and after exponential subtraction with RESA, the intensity of the marker is divided into the subcellular compartments by pixel-based locale assignment for compartmentalization of expression (PLACE algorithm). An AQUA score (intensity/area) is generated for the target within the subcellular compartments. This information is graphically represented by the target localization image.



with longer disease-free and overall survival. The quantitative assay we describe in this work confirms and extends these observations.

MATERIALS AND METHODS

Tissue Microarray Construction. The tissue microarray was constructed as previously described (28, 29). A total of 570 tissue cores representing 542 total melanoma cases and a small series of controls measuring 0.6 mm were spaced 0.8 mm apart on a single glass slide. The cohort was constructed from formalin-fixed, paraffin-embedded tissue blocks obtained from the archives of the Department of Pathology at Yale University School of Medicine. A pathologist examined each case to select the region for inclusion in the tissue microarray. Core biopsies from the specimens were placed on the tissue microarray with a Tissue Micorarrayer (Beecher Instruments, Sun Prairie, WI). The tissue microarrays were then cut to 5- μm sections and placed on glass slides with the adhesive tape transfer system (Instumedics, Inc., Hackensack, NJ) with UV cross-linking. The specimens were all drawn from archives of tumors resected between 1959 and 1994, with a follow-up range of 2 months and 38 years (median follow-up time, 60 months). The cohort characteristics are demonstrated in Table 1. For the primary cutaneous lesions (269), a single reviewer measured Breslow depth, Clark level, microscopic satellites, tumor-infiltrating lymphocytes, and the presence of ulceration. Treatment information was not available for the entire cohort. Some of the stage III patients were treated with IFN-based therapy, and the stage IV patients were treated with a range of therapies, including chemotherapy, biological therapy, vaccine therapy, and supportive care.

Immunohistochemistry. The tissue microarray slide was stained as described previously (16). In brief, the slides were deparaffinized by rinsing with xylene, followed by two changes of 100% ethanol and two changes of 95% ethanol. Antigen retrieval was performed in a pressure cooker containing 1 mmol/L EDTA (pH 7.5), and endogenous peroxidase activity was blocked with 2.5% hydrogen peroxide in methanol for 30 minutes at room temperature. The slide was washed with Tris-buffered saline (TBS), incubated in 0.3% BSA/1 \times TBS for 30 minutes at room temperature to reduce nonspecific background, and then stained with the a combination of anti-MDM2 mouse monoclonal antibody 1B10 (1:100, Novocastra, Ltd., Newcastle upon Tyne, United Kingdom) plus anti-S100 rabbit polyclonal (1:6000, DAKO Corporation, Carpinteria, CA) diluted in BSA/TBS at 4 $^{\circ}\text{C}$ overnight. The 1B10 monoclonal antibody was chosen because it was validated by numerous studies in which HDM2 expression was assessed in tumors relative to normal tissues (30–32). The secondary antibodies Alexa 488-conjugated goat antirabbit (1:100, Molecular Probes, Eugene, OR) plus Envision antimouse (neat; DAKO)

diluted in BSA/TBS were applied for 1 hour at room temperature. 4',6-Diamidino-2-phenylindole was included with the secondary antibodies to visualize nuclei. The slide was washed with BSA/TBS (three times for 5 minutes) and then incubated with Cy5-tyramide (Perkin-Elmer Life Science Products, Boston, MA) and activated by horseradish peroxidase, resulting in the deposition of numerous covalently associated Cy5 dyes immediately adjacent to the horseradish peroxidase-conjugated secondary antibody. Cy5 was used because its emission peak (red) is well outside of the green-orange spectrum of tissue autofluorescence. The slides were sealed with coverslips with an antifade-containing mounting medium (with 0.6% *n*-propyl gallate).

Automated Image Acquisition and Analysis. The AQUA automated image acquisition and analysis was performed as described previously (16). Briefly, images of the tissue microarray were captured through an Olympus BX51 microscope with automated *x*, *y*, and *z* stage movement with an Olympus Motorized Reflected Fluorescence System and software (IP lab v3.54, Scanalytics, Inc., Fairfax, VA) equipped with Cooke Sensicam QE High Performance camera. Low-power images of the microarray were stitched together with multiple low-resolution images of the microarray (64 \times 64 pixel) at $\sim 7\text{-}\mu\text{m}$ resolution. Histospots were identified with the signal from 4',6-diamidino-2-phenylindole and/or S100 tags. Rows and columns of the histospots were then identified, missing histospots filled in, allowing each histospot to be identified by its coordinates, and recorded based on its position in the grid. Subsequently, monochromatic, high-resolution (1024 \times 1024 pixel, 0.5- μm resolution) images were obtained of each histospot, both in the plane of focus, and 8 μm below it, and recorded in an image stack as bitmaps. A resolution of 0.5 μm is suitable for distinguishing between large subcellular compartments such as the cell membrane/cytoplasm and nuclei. Images were obtained with a pixel intensity dynamic range of 0 to 255.

Table 1 Tissue microarray characteristics

Primary Lesions (287)
269 Cutaneous
18 Mucosal
Metastatic Lesions (233)
118 Lymph node
65 Cutaneous & subcutaneous
11 Lung
8 Bone
2 Brain
26 Other distant
3 Unknown
Local Recurrences (20)
Unknown (2)

A visual demonstration of the AQUA process is depicted in Fig. 1. For each histospot, areas of tumor are distinguished from stromal elements by creating a tumor mask from the S100 protein signal visualized under the Alexa 488 fluorophore. The tumor mask is determined by gating the pixels in this image in which an intensity threshold is set by visual inspection of histospots (ranging from lowest to highest intensity), and each pixel is recorded as “on” (tumor) or “off” (nontumor) based on the threshold. In addition, small objects (<50 pixels) are removed and small holes filled. The 4',6-diamidino-2-phenylindole image, used to identify the nuclei, is subjected to rapid exponential subtraction algorithm, which improves signal-to-noise ratio by subtracting the out-of-focus image from the in-focus image to clearly define the nuclear compartment (16). Removal of the pixels assigned to the nuclear compartment from the tumor mask provides a designation of the cytoplasmic compartment. After application of rapid exponential subtraction algorithm, the signal intensity of the target antigen, acquired under the Cy5 signal (HDM2), is scored on a scale of 0 to 255, and the AQUA score within the subcellular compartments (*i.e.*, nucleus, cytoplasm) is calculated by dividing signal intensity by the area of the specified compartment. This score has three significant figures and is directly proportional to the number of molecules per unit area.

Data Analysis. Histospots containing <10% tumor as assessed by mask area were excluded from further analysis. Previous studies have demonstrated that the staining from a single histospot provides sufficient representative sample to judge outcomes (33, 34). In the case of HDM2, staining was always nuclear; analyses using the nuclear-specific automated quantitative analysis score of HDM2 yielded parallel results to analyses using the total automated quantitative analysis score. Univariate survival analyses were assessed using

the Kaplan-Meier method for nominal variables and the Cox regression method for continuous variables. Multivariate analyses were performed with the Cox proportional hazards model. Mantel-Cox log-rank score was used to assess statistical significance. Analyses were performed with JMP 5.0.1 (SAS Institute, Inc., Cary, NC). Patients were deemed uncensored if they died of melanoma within 30 years of their initial date of diagnosis.

RESULTS

Validation of Microarray Cohort. We sought to validate our tissue microarray cohort of 542 melanomas with several traditional histopathological markers of malignancy. As previously described (28) and demonstrated in Table 1, unique patient-specific cases on the tissue microarray include 287 primary specimens, 233 metastatic specimens, and 20 local recurrences. Using univariate analysis of long-term disease-related survival, primary *versus* metastatic status predicted improved survival ($P < 0.0001$; Fig. 2A) For the primary cutaneous specimens, we found that tumor depth (Breslow and Clark; $P < 0.0001$), ulceration status ($P = 0.0028$), microscopic satellitosis ($P < 0.0001$), tumor-infiltrating lymphocytes ($P = 0.0007$), and histologic subtype were all significant predictors of survival (Fig. 2B–F).

Automated Analysis of HDM2 Expression in Melanoma. After image acquisition for each histospot, automated quantitative analysis

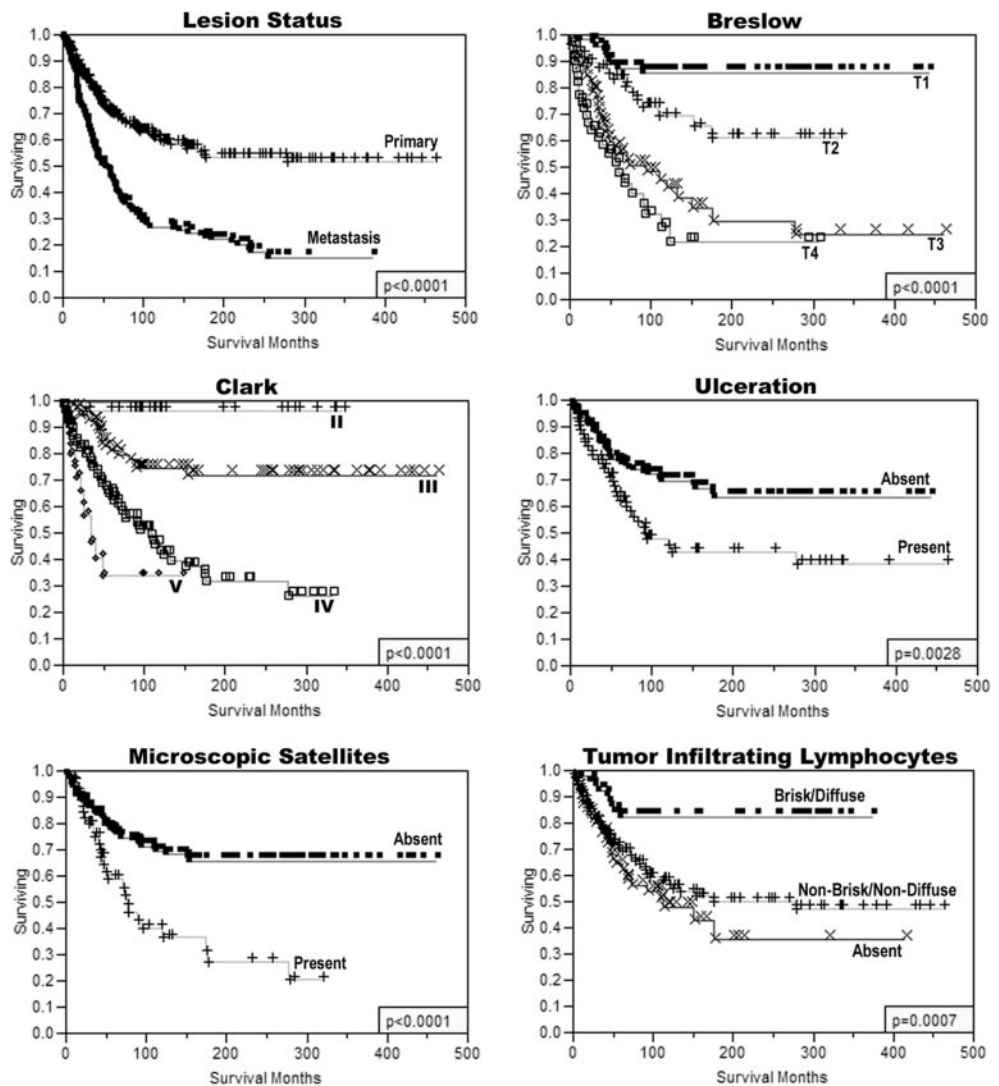


Fig. 2. Melanoma tissue microarray characteristics. Kaplan-Meier survival curves demonstrating disease-specific survival based on lesion location (*i.e.*, primary *versus* metastatic), as well as the role of standard histopathological criteria on survival in this cohort, which includes Breslow depth (T1–T4), Clark levels (II–V), the presence or absence of ulceration, the presence or absence of microscopic satellites, and presence of infiltrating lymphocytes.

was performed to establish the intensity of HDM2 expression per unit area within each histospot (Fig. 1). HDM2 expression was confined to the cell nuclei, and analysis of AQUA scores of HDM2 within the nuclear compartment yielded similar results to analysis of HDM2 expression within the overall tumor mask, suggesting nearly all of the expression is in the nucleus.

AQUA score calculation results in a continuous scale in contrast to manual scoring, which is based on an ordinal scale with arbitrary values. Regression analysis has previously demonstrated a good correlation between the two methods (16, 17). Of the 542 total histospots, 405 contained sufficient tumor tissue to provide an automated quantitative analysis score for HDM2. The loss of histospots is random but reduces the number of cases available for analysis in the remainder of this study. Of the 405 cases analyzed, 200 were primary lesions and 190 were metastases, 13 were local recurrences, and 2 were of unknown origin. AQUA scores in the melanoma-specific nuclear compartment of all specimens ranged from 19.62 to 150.72 and from 21.84 to 145.98 within nuclear compartment of primary lesions. The histogram in Fig. 3A demonstrates the continuous nature and bell-shaped distribution of the AQUA scores for all of the specimens. Note that in other systems, we have evidence that the scores are directly proportional to the number of molecules per unit area. This is probably also true for HDM2, but purified protein standard controls were not available to validate this prediction.

HDM2 expression in the primary lesions was compared with expression in cutaneous metastases, lymph node metastases, and distant metastases. Fig. 3B shows that loss of HDM2 is more common in later-stage disease. This may be related to specific classes of tumor with low expression having a great propensity for progression. The significance of the difference between the means of the AQUA scores for each tissue type (*i.e.*, skin metastases, lymph node metastases, distant metastases) from the AQUA scores of primary lesions was determined by *t* tests, demonstrated in the Table 2.

Survival Analysis. Because the AQUA scores are of a continuous nature, the HDM2 expression scores were analyzed by univariate Cox regression. This univariate parametric survival analysis demonstrated that high HDM2 expression was associated with improved survival in all specimens ($P = 0.0154$) and in the primary lesions alone ($P = 0.0318$). However, when HDM2 expression was evaluated in only the metastatic specimens, it did not show a significant association with survival ($P = 0.9330$). To graphically depict the influence of HDM2 on survival in melanoma, the scores were divided into quartiles, and Kaplan-Meier survival curves were constructed for HDM2 expression. The *P* values for these curves were determined by the Mantel-Cox log-rank method. Assessment of survival in all specimens demonstrated that high expression of HDM2 is associated with better disease-specific survival ($P = 0.0382$; Fig. 3C). Examination of HDM2 expression in relation to survival in only the primary specimens followed the same trend, revealing improved outcome for high expressers ($P = 0.0211$; Fig. 3D). The quartile cutpoints established for AQUA scores in all specimens were maintained in evaluation of the primary lesions.

Clinicopathologic Correlations. Table 2 and Fig. 3B demonstrate that decreased expression of HDM2 is associated with metastasis. Within primary lesions, there is a relationship between HDM2 expression and lesion progression. Table 3 demonstrates that HDM2 exhibits an association with Breslow thickness, Clark level, and tumor-infiltrating lymphocytes but not with microscopic satellites, ulceration, primary tumor location, age, or sex. Cases missing clinical data are excluded from statistical analysis (labeled unknown). These data indicate that HDM2 expression decreases as lesions progress

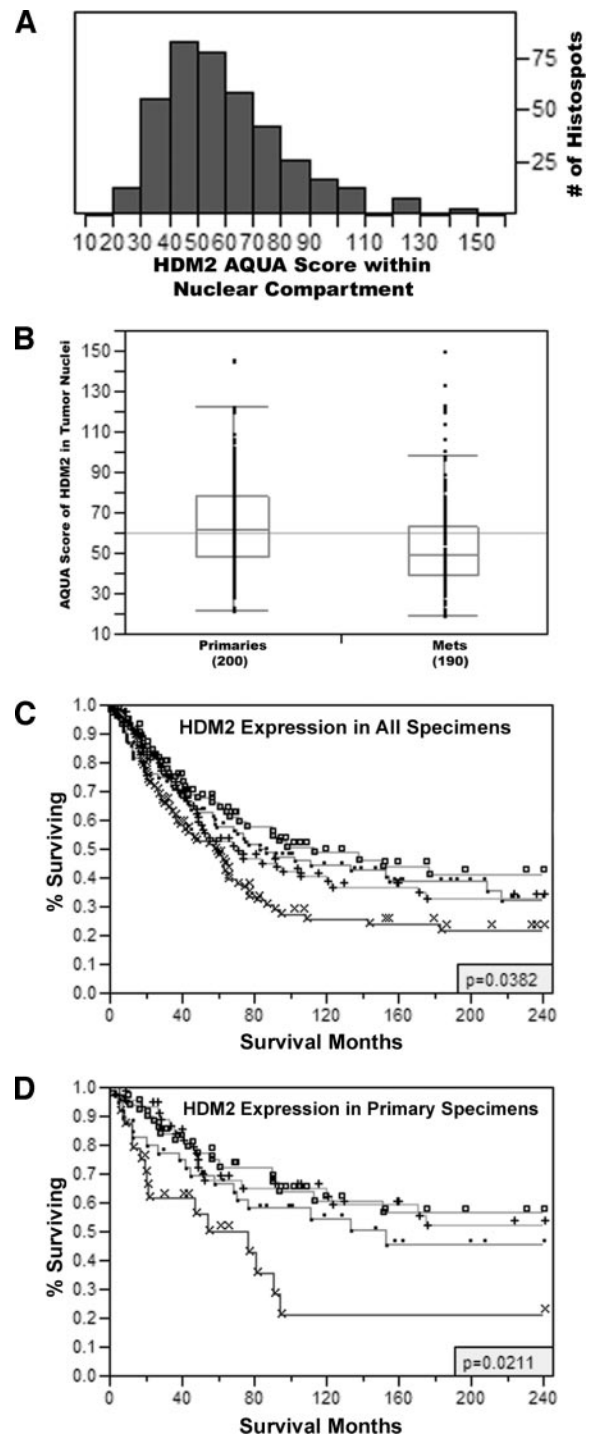


Fig. 3. A, HDM2 protein expression histogram for AQUA analysis within the nuclear compartment of the tumor mask. The histogram demonstrates the ability of automated quantitative analysis (AQUA) to give a continuous readout of HDM2 protein expression. B, one-way analysis of AQUA scores demonstrating significantly higher levels of HDM2 in primary melanoma compared with metastatic lesions (mets). Additional stratification (primary, cutaneous metastases, lymph node metastases, and distant metastases) demonstrates that there is a significant decrease in HDM2 expression as lesions progress to more advanced stages (refer to Table 2). C, Kaplan-Meier survival plot of HDM2 expression in all specimens based on AQUA score demonstrating stratification by quartiles. D, Kaplan-Meier survival plot of HDM2 expression in only the primary lesions. For C and D: \times , bottom 25%; \bullet , 25 to 50%; $+$, 50 to 75%; and \square , top 25%.

deeper into the dermis (Breslow thickness and Clark level). Multivariate analysis revealed that HDM2 is not independently predictive presumably because of its tight association with variables defining depth of invasion (data not shown).

Table 2 HDM2 protein expression within tumor nuclei by AQUA analysis

	n	Mean	SE	95% confidence interval	Comparison with mean of primaries				
					Difference	SE	t test	DF	P
Primaries	200	65.73	1.57	62.63–68.83					
Skin metastases	52	58.37	3.24	51.98–64.76	7.36	3.64	2.02	250	0.0445
Lymph node metastases	98	53.72	2.28	49.23–58.21	12.01	2.78	4.31	296	<0.0001
Distant metastatic tumor	40	49.22	3.52	42.28–56.15	16.51	3.86	4.28	238	<0.0001
All metastatic tumor	190	54.05	1.63	50.85–57.24	11.68	2.27	5.15	388	<0.0001

DISCUSSION

HDM2 overexpression correlated positively with poor prognosis in sarcoma, glioma, and pediatric acute lymphocytic leukemia but negatively for non-small-cell lung cancer, estrogen receptor α -positive breast carcinoma, and melanoma (reviewed in ref. 24). Pathologist-based, traditional analysis of HDM2 expression in a melanoma cohort of 134 patients demonstrated that HDM2 overexpression was unexpectedly associated with improved survival (27). The method of scoring used by Polsky *et al.* (27) was based on a scale of nuclear immunoreactivity, ranging from undetectable (0%) to homogeneous staining (100%). Their choice of cutpoint was based on prior experience with this antibody in other cancers (*i.e.*, bladder, prostate, squamous cell carcinomas, and sarcomas) in which the 20% cutpoint-stratified patients in a clinically relevant fashion, but they acknowledged that the appropriate cutpoints for cutaneous melanoma remain to be established (27).

The continuous nature of AQUA scores makes it difficult to determine a cutpoint for survival analyses; however, expression of HDM2 diminished as lesions became more invasive (Tables 2 and 3 and Fig. 3B). Therefore, the AQUA scores of HDM2 expression were stratified into quartiles, and survival curves were plotted to predict outcome. In concordance with Polsky *et al.* (27), we also found that high expression of HDM2 predicted a favorable prognosis (Fig. 3C). The ability to predict survival was more apparent when the analysis was limited to primary lesions (Fig. 3D).

The apparent paradox of HDM2 overexpression having a protective effect was suggested to indicate the presence of a functional p53 exerting an inhibitory effect on tumor proliferation and activating the HDM2 promoter as part of its normal autoregulatory feedback loop (27). The p53 tumor suppressor plays a critical role in the cellular response to DNA damage, preventing altered, premalignant cells from progressing to cancer. In response to DNA damage, the p53 protein initiates a variety of stress-specific transcriptional response programs that lead to growth arrest, apoptosis, or senescence (21). In addition to inducing these response programs, p53 also tightly regulates its own intracellular level via an autoregulatory feedback loop with HDM2. Transcription of HDM2 is stimulated by p53, and HDM2, in turn, directly ubiquitinates p53 and targets it to proteasomal degradation (23). Recent experiments by Lahav *et al.* (35) on the dynamics of the p53-MDM2 feedback loop demonstrate that this negative feedback system functions in a digital fashion in which expression of repair enzymes occurs in defined linear quanta rather than a binary switch-like (all-or-nothing) response. Cells probably express frequent pulses of HDM2 induction when exposed to damage, and histologic sections may represent a snapshot of this dynamic result. That is, a set of cells undergoing pulses that are more frequent would be more likely to be expressing HDM2 at the time of excision and fixation.

However, in light of all of the examples demonstrating the regulatory functions of MDM2/HDM2 on p53, there is mounting evidence demonstrating p53-independent functions of HDM2 (36). This protein has been shown to interact with multiple factors (*e.g.*, ARF, MDMX, ATM, c-abl, HIF-1 α , RB, PML, E2F) that can play a role in transformation, affecting cell cycle control, differentiation, DNA synthesis,

RNA biosynthesis, transcription, and cell surface receptor turnover (37). As with p53, which plays roles in both transcriptional regulation and mediation of apoptosis in mitochondria (38), HDM2 may also have a second role, unrelated to its interaction with p53. It should also be noted that a number of other oncoproteins such as Ras (39, 40), Raf-1 (41), and Bcl-2 (42) have recently been shown to possess secondary, growth inhibitory functions. These dual-function oncoproteins, including HDM2, may be essential to the proliferation of normal cells equipped with growth suppressor activities that have not been fully characterized (43).

The AQUA system provides a unique method for the analysis of tissue microarrays not previously possible with standard pathologist-based techniques. The system is precise, highly reproducible, and quantitative resulting in continuous measurements similar to that obtained from ELISA assays. In addition, automated quantitative analysis allows for accurate subcellular localization, with the ability to discriminate between the cytoplasmic and nuclear compartments in melanoma cells. With increased resolution, the analyses will expand to include additional virtual compartments (*e.g.*, mitochondria, lyso-

Table 3 HDM2 expression and clinicopathologic features of primary lesions

Factor	HDM2 expression within tumor nuclei (quartiles)				P
	Bottom 25% (n = 31) No. (%)	25–50% (n = 48) No. (%)	50–75% (n = 55) No. (%)	Top 25% (n = 66) No. (%)	
Breslow thickness					
≤1 mm (T1)	0 (0)	10 (17.9)	16 (28.6)	30 (53.6)	<0.0001
1.01–2.0 mm (T2)	7 (15.6)	10 (22.2)	15 (33.3)	13 (28.9)	
2.01–4 mm (T3)	9 (18.8)	16 (33.3)	13 (27.1)	10 (20.8)	
≥4 mm (T4)	12 (30.8)	9 (23.1)	8 (20.5)	10 (25.6)	
Unknown	3	3	3	3	
Clark level					
I	0 (0)	0 (0)	0 (0)	0 (0)	0.0029
II	0 (0)	0 (0)	8 (38.1)	13 (61.9)	
III	10 (14.7)	19 (27.9)	18 (26.5)	21 (30.9)	
IV	14 (17.5)	19 (23.8)	23 (28.8)	24 (30)	
V	3 (15)	8 (40)	4 (20)	5 (25)	
Unknown	4	2	2	3	
TILs					
Brisk/Diffuse	1 (2.1)	11 (23.4)	14 (29.8)	21 (44.7)	0.0392
Nonbrisk/Nondiffuse	20 (20.2)	26 (26.3)	26 (26.3)	27 (27.3)	
Absent	7 (16.3)	9 (21.0)	13 (30.2)	14 (32.6)	
Unknown	3	2	2	4	
Age (y)					
<60	9 (8.9)	27 (26.7)	30 (29.7)	35 (34.7)	0.1797
≥60	17 (20.2)	20 (23.8)	22 (26.2)	25 (29.8)	
Unknown	5	1	3	6	
Ulceration					
Present	12 (20.3)	15 (25.4)	17 (28.8)	15 (25.4)	0.2585
Absent	14 (11.4)	28 (22.8)	35 (28.5)	46 (37.4)	
Unknown	5	5	3	5	
Sex					
Male	12 (14.3)	19 (22.6)	27 (32.1)	26 (31.0)	0.5304
Female	15 (15.3)	25 (25.5)	22 (22.5)	36 (36.7)	
Unknown	4	4	6	4	
Microscopic satellites					
Present	7 (18.0)	9 (23.1)	8 (20.5)	15 (38.5)	0.5535
Absent	19 (13.5)	33 (23.4)	44 (31.2)	45 (31.9)	
Unknown	5	6	3	6	
Primary tumor location					
Axial	12 (15)	20 (25)	24 (30)	24 (30)	0.5701
Extremity	9 (9.5)	26 (27.4)	25 (26.3)	35 (36.8)	
Unknown	10	2	6	7	

somes, endoplasmic reticulum, Golgi, and so forth). The system has been effectively demonstrated on colon (16), breast (17), and prostate (18) carcinomas. The automated nature of this technology can allow high-throughput screening of tissue microarrays, facilitating their use in discovery of chemotherapeutic targets and biomarker validation.

In summary, AQUA-based analysis was used to demonstrate that HDM2 is a marker of melanoma progression. As might be expected of a marker of progression, it is also useful for prognostication independent of all conventional histologic markers, except those related to tumor depth of invasion. In primary lesions, this biomarker may represent a mechanism to predict survival in a tumor type without standard molecular tools for prediction of outcome.

REFERENCES

- Rigel DS, Friedman RJ, Kopf AW. The incidence of malignant melanoma in the United States: issues as we approach the 21st century. *J Am Acad Dermatol* 1996; 34:839–47.
- Ries LAG, Eisner MP, Kosary CL, et al. SEER cancer statistics review, 1975–2001. Vol. 2004. Bethesda, MD: National Cancer Institute; 2004.
- Jemal A, Murray T, Samuels A, et al. Cancer statistics, 2003. *CA - Cancer J Clin* 2003;53:5–26.
- Weinstock MA. Do sunscreens increase or decrease melanoma risk: an epidemiologic evaluation. *J Invest Dermatol Symp Proc* 1999;4:97–100.
- Jemal A, Thomas A, Murray T, Thun M. Cancer statistics, 2002. *CA - Cancer J Clin* 2002;52:23–47.
- Bittner M, Meltzer P, Chen Y, et al. Molecular classification of cutaneous malignant melanoma by gene expression profiling. *Nature (Lond.)* 2000;406:536–40.
- Breslow A. Thickness, cross-sectional areas and depth of invasion in the prognosis of cutaneous melanoma. *Ann Surg* 1970;172:902–8.
- Clark WH Jr, Ainsworth AM, Bernardino EA, et al. The developmental biology of primary human malignant melanomas. *Semin Oncol* 1975;2:83–103.
- Balch CM, Buzaid AC, Soong SJ, et al. Final version of the American Joint Committee on Cancer staging system for cutaneous melanoma. *J Clin Oncol* 2001; 19:3635–48.
- Alonso SR, Ortiz P, Pollan M, et al. Progression in cutaneous malignant melanoma is associated with distinct expression profiles: a tissue microarray-based study. *Am J Pathol.* 2004;164:193–203.
- Korabiowska M, Bauer H, Quentin T, et al. Application of new in situ hybridization probes for Ku70 and Ku80 in tissue microarrays of paraffin-embedded malignant melanomas: correlation with immunohistochemical analysis. *Hum Pathol* 2004;35: 210–6.
- Taylor CR. The total test approach to standardization of immunohistochemistry. *Arch Pathol Lab Med* 2000;124:945–51.
- Thomson TA, Hayes MM, Spinelli JJ, et al. HER-2/neu in breast cancer: interobserver variability and performance of immunohistochemistry with 4 antibodies compared with fluorescent in situ hybridization. *Mod Pathol* 2001;14:1079–86.
- Kay EW, Walsh CJ, Cassidy M, Curran B, Leader M. C-erbB-2 immunostaining: problems with interpretation. *J Clin Pathol (Lond.)* 1994;47:816–22.
- Kononen J, Bubendorf L, Kallioniemi A, et al. Tissue microarrays for high-throughput molecular profiling of tumor specimens. *Nat Med* 1998;4:844–7.
- Camp RL, Chung GG, Rimm DL. Automated subcellular localization and quantification of protein expression in tissue microarrays. *Nat Med* 2002;8:1323–7.
- Camp RL, Dolled-Filhart M, King BL, Rimm DL. Quantitative analysis of breast cancer tissue microarrays shows that both high and normal levels of HER2 expression are associated with poor outcome. *Cancer Res* 2003;63:1445–8.
- Rubin MA, Zerkowski MP, Camp RL, et al. Quantitative determination of expression of the prostate alpha-methylacyl-CoA racemase using automated quantitative analysis (AQUA): a novel paradigm for automated and continuous biomarker measurements. *Am J Pathol* 2004;164:831–40.
- Smoller BR. Immunohistochemistry in the diagnosis of melanocytic neoplasms. *Pathology (Phila.)* 1994;2:371–83.
- Dabbs DJ. *Diagnostic immunohistochemistry*. 1st ed. Philadelphia: Churchill Livingstone; 2002.
- Vogelstein B, Lane D, Levine AJ. Surfing the p53 network. *Nature (Lond.)* 2000; 408:307–10.
- Michael D, Oren M. The p53-Mdm2 module and the ubiquitin system. *Semin Cancer Biol* 2003;13:49–58.
- Piette J, Neel H, Marechal V. Mdm2: keeping p53 under control. *Oncogene* 1997; 15:1001–10.
- Onel K, Cordon-Cardo C. MDM2 and prognosis. *Mol Cancer Res* 2004;2:1–8.
- Hernberg M, Turunen JP, von Boguslawsky K, Muhonen T, Pyrhonen S. Prognostic value of biomarkers in malignant melanoma. *Melanoma Res* 1998;8:283–91.
- Sauroja I, Smeds J, Vlaykova T, et al. Analysis of G₁-S checkpoint regulators in metastatic melanoma. *Genes Chromosomes Cancer* 2000;28:404–14.
- Polsky D, Melzer K, Hazan C, et al. HDM2 protein overexpression and prognosis in primary malignant melanoma. *J Natl Cancer Inst (Bethesda)* 2002;94:1803–6.
- Berger AJ, Kluger HM, Li N, et al. Subcellular localization of activating transcription factor 2 in melanoma specimens predicts patient survival. *Cancer Res* 2003;63: 8103–7.
- Rimm DL, Camp RL, Charette LA, et al. Tissue microarray: a new technology for amplification of tissue resources. *Cancer J* 2001;7:24–31.
- Matsumura T, Yoshihama Y, Kimura T, Shintani S, Alcalde RE. p53 and MDM2 expression in oral squamous cell carcinoma. *Oncology* 1996;53:308–12.
- Piotti S, Della Torre G, Lavarino C, et al. Distinct mdm2/p53 expression patterns in liposarcoma subgroups: implications for different pathogenetic mechanisms. *J Pathol* 1997;181:14–24.
- Higashiyama M, Doi O, Kodama K, et al. MDM2 gene amplification and expression in non-small-cell lung cancer: immunohistochemical expression of its protein is a favourable prognostic marker in patients without p53 protein accumulation. *Br J Cancer* 1997;75:1302–8.
- Camp RL, Charette LA, Rimm DL. Validation of tissue microarray technology in breast carcinoma. *Lab Invest* 2000;80:1943–9.
- Torhorst J, Bucher C, Kononen J, et al. Tissue microarrays for rapid linking of molecular changes to clinical endpoints. *Am J Pathol.* 2001;159:2249–56.
- Lahav G, Rosenfeld N, Sigal A, et al. Dynamics of the p53-Mdm2 feedback loop in individual cells. *Nat Genet* 2004;36:147–50.
- Ganguli G, Wasyluk B. p53-independent functions of MDM2. *Mol Cancer Res* 2003;1:1027–35.
- Iwakuma T, Lozano G. MDM2, an introduction. *Mol Cancer Res* 2003;1:993–1000.
- Moll UM, Zaika A. Nuclear and mitochondrial apoptotic pathways of p53. *FEBS Lett* 2001;493:65–9.
- Ferbeyre G, de Stanchina E, Lin AW, et al. Oncogenic ras and p53 cooperate to induce cellular senescence. *Mol Cell Biol* 2002;22:3497–508.
- Serrano M, Lin AW, McCurrach ME, Beach D, Lowe SW. Oncogenic ras provokes premature cell senescence associated with accumulation of p53 and p16INK4a. *Cell* 1997;88:593–602.
- Olsen CL, Gardie B, Yaswen P, Stampfer MR. Raf-1-induced growth arrest in human mammary epithelial cells is p16-independent and is overcome in immortal cells during conversion. *Oncogene* 2002;21:6328–39.
- O'Reilly LA, Huang DC, Strasser A. The cell death inhibitor Bcl-2 and its homologues influence control of cell cycle entry. *EMBO J* 1996;15:6979–90.
- Deb SP. Cell cycle regulatory functions of the human oncoprotein MDM2. *Mol Cancer Res* 2003;1:1009–16.